IEEE Access
Multidisciplinary | Rapid Review | Open Access Journal

Received November 14, 2019, accepted December 4, 2019, date of publication December 10, 2019,
date of current version December 23, 2019.

Digital Object Identifier 10.1109/ACCESS.2019.2958745

Dual-Band Ten-Element MIMO Array Based on Dual-Mode IFAs for 5G Terminal Applications

WEI HU[1], (Member, IEEE), XUEKANG LIU[1], STEVEN GAO[2], (Fellow, IEEE), LE-HU WEN[2], LONG QIAN[1], TIANXI FENG[1], RUI XU[2], PENG FEI[3], AND YING LIU[1], (Senior Member, IEEE)

[1]National Laboratory of Science and Technology on Antennas and Microwaves, Xidian University, Xi'an 710071, China
[2]School of Engineering and Digital Arts, University of Kent, Canterbury CT2 7NT, U.K.
[3]Beijing Institute of Radio Metrology and Measurement, Beijing 100854, China

Corresponding authors: Wei Hu (weihu.xidian@ieee.org) and Xuekang Liu (hcmx1994@gmail.com)

This work was supported in part by the Young Talent Fund of University Association for Science and Technology in Shaanxi, China, under Grant 20170105, in part by the Natural Science Foundation of Shaanxi, China, under Grant 2018JM6038, in part by the Engineering and Physical Sciences Research Council (EPSRC) under Grant EP/N032497/1, Grant EP/P015840/1, and Grant EP/S005625/1, and in part by the Fundamental Research Funds for the Central Universities under Grant RC1902.

ABSTRACT A dual-band ten-element MIMO array based on dual-mode inverted-F antennas (IFAs) for 5G terminal applications is presented in this paper. The proposed dual-mode IFA is composed of two radiators, which are etched on the outer and inner surfaces of the side-edge frame. The outer part of the antenna generates the low-order mode at 3.5 GHz, while the inner part radiates another one-quarter-wavelength mode at 4.9 GHz. In this way, the IFA can achieve dual-band operation within a compact size of $10.6 \times 5.3 \times 0.8$ mm^3. Based on the proposed antenna, a dual-band ten-element multiple-input and multiple-output (MIMO) array is developed for 5G terminal applications. By combining neutralization line structures with decoupling branches, the isolations between the elements are improved. To validate the design concept, a prototype of the ten-element MIMO array is designed, fabricated, and measured. The experimental results show that the proposed antenna can cover the 3.3-3.6 GHz and 4.8-5.0 GHz bands with good isolation and high efficiency. Furthermore, the envelope correlation coefficient (ECC), and channel capacity are also calculated to verify the MIMO performances for 5G sub-6GHz applications.

INDEX TERMS Dual-band antenna, dual-mode IFA, fifth generation (5G) communication, MIMO antenna.

I. INTRODUCTION

In recent years, to meet the increasing requirements of high communication capacity, low time delay, and massive connection density, the fifth-generation (5G) mobile communication system with multi-band, high isolation and ergodic channel capacity is in urgent need. As one of the most significant technologies in 5G system, the MIMO technology has become a research hotspot. Recently, several four-element MIMO arrays for terminal applications working at the sub-6 GHz band have been reported in [1]–[4]. However, these four-element MIMO arrays showed the relatively low channel capacity due to the small number of antenna elements.

To improve the upper performance of MIMO systems, many eight-element MIMO arrays have been reported recently. In [5]–[12], eight-element MIMO arrays were designed to cover the long-term evolution (LTE) band 42 (3.4-3.6 GHz). By using eight monopoles as the elements, a MIMO array with good ergodic channel capacity of 40 bps/Hz was presented in [5]. However, this design suffered from low isolation between the antenna elements. In [7], a combined design of two types of four-element arrays (U-shaped and L-shaped loop elements) were proposed for the LTE 42 band 5G application. By employing hybrid decoupling structures, 15 dB isolations were obtained. In [9]–[12], eight-element MIMO arrays with good isolations better than 15 dB within 3.4-3.6 GHz band have been reported. Nevertheless, large element sizes of these antenna arrays limit their applications in higher order MIMO arrays.

In order to meet the demands of modern terminal devices for multi-standard compatibility, dual-band and broad-band eight-element MIMO arrays were proposed in [13]–[17].

The associate editor coordinating the review of this manuscript and approving it for publication was Luyu Zhao.

In [14], an eight-port antenna array was presented to cover the LTE band 42 and 4.9-GHz band (4.8–5.1 GHz) for the 5G MIMO. The array is in a compact size at the expense of the low isolation. By using eight L-shaped slot antennas based on stepped impedance resonators (SIRs), a dual-band eight-antenna array was proposed to work at the LTE band 42 and LTE band 46 (5.15-5.93 GHz) in [15]. Although eight-element MIMO array has a higher upper limit of ergodic channel capacity (46 bps/Hz with a 20-dB signal-to-noise ratio (SNR)) compared with four-element MIMO array (23 bps/Hz with a 20-dB SNR). The ergodic channel capacity still can be improved by increasing the element number of the MIMO array.

To further enhance the upper limit of ergodic channel capacity within the existing bandwidth, ten-element MIMO array, twelve-element MIMO array, even sixteen-element MIMO array have been presented in [18]–[21]. In [19], a sixteen-element MIMO which covers single band (3.4-3.6 GHz) was reported. The calculated channel capacity of the array can reach up to 66-70 bps/Hz with a 20-dB SNR. But it suffered from low isolation and low efficiency. A ten-element MIMO array in [21] was designed to realize multi-band (LTE bands 42/43 and LTE band 46) coverage. However, unlike the arrangement along the long side, the antenna elements are placed around the ground plane, which will increase the design complexity of 2G/3G/4G antennas.

In this paper, a dual-band ten-element MIMO array based on dual-mode IFAs is proposed for 5G terminal applications. The dual-mode IFA is composed of two parts which etched on the outer and inner surface of the side-edge frame, respectively. This IFA element is designed with two different resonant modes in a compact size. The outer part resonates at around 3.5 GHz, while the inner part generates a resonant mode at about 4.9 GHz. Based on the dual-mode IFA, a ten-element antenna array is developed for 5G smartphone application. Additionally, to enhance the isolation between the adjacent elements, decoupling branches and neutralization lines are introduced. In order to verify the design concept, the proposed MIMO array is manufactured, and tested. The experimental results, such as S-parameters, antenna efficiencies, and radiation patterns are given for verification. The envelope correlation coefficient (ECC), and channel capacity are also calculated to verify the MIMO performances. Finally, to evaluate the robustness of the antenna performances, the user's hand effects are also studied.

II. ANTENNA CONFIGURATION

The detailed design and geometrical configuration of the proposed dual-band ten-element MIMO array for the 5G smartphone application are shown in Fig. 1. The dimension of the system circuit board is $150 \times 70 \times 0.8\text{mm}^3$, which is a typical dimension for a 5.5-inch handset. Two clearance areas ($70 \times 5\text{mm}^2$) that are located separately at the top and bottom end of the system circuit board are reserved for the current 2G/3G/4G LTE smartphone antennas. Two side-edge

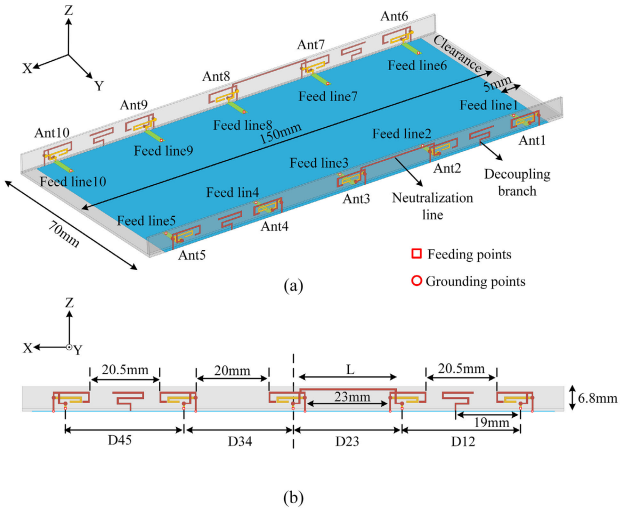

FIGURE 1. Configuration of the proposed ten-element array. (a) Overall view. (b) Side view.

frames with a width of 6 mm are chosen for a slim smartphone requirement. The ten antenna elements, which are printed on the two side-edge frames, are placed perpendicularly to the system substrate. Each side-edge frame is printed with five antenna elements. The five-element array located at each side-edge frame is composed of a single antenna element in the middle and two antenna pairs in the both sides. The two antenna pairs at the right side-edge frame are (Ant1, Ant2) and (Ant4, Ant5), while those at the left side-edge frame are (Ant6, Ant7) and (Ant 9, Ant 10). Ant3 and Ant8 are located at the center of the right and left side-edge frames, respectively. Each antenna element in the proposed MIMO array is a dual-mode IFA with the same dimension of 10.6×5.3 mm^2 ($0.12\lambda \times 0.06\lambda$, where λ is the free space wavelength at 3.5 GHz). Four decoupling branches with the length of about a quarter wavelength at 3.5 GHz are etched between the antenna pairs to enhance the isolation between the two adjacent elements, and two neutralization lines are introduced between Ant2 and Ant3, and Ant7 and Ant8. The distances between the antenna elements are D12=D45=34 mm and D23=D34=30.1 mm. The whole MIMO antenna system is designed on the FR4 substrates (relative dielectric permittivity $\varepsilon_r = 4.4$, loss tangent $\tan\delta = 0.02$).

III. TEN-ELEMENT MIMO ARRAY DESIGN

The design of the dual-band ten-element MIMO array is presented in this section. First, the dual-band operation mechanism of the proposed dual-mode IFA antenna element is investigated. Then, based on the dual-mode IFA, a ten-element antenna array is developed for 5G smartphone application. Finally, to improve the isolations between the adjacent elements, decoupling branches and neutralization lines are introduced in the design.

A. DUAL-MODE IFA ELEMENT

Fig. 2 shows the detailed dimensions and structure of the dual-mode IFA element, which is a dual-branch IFA fed at

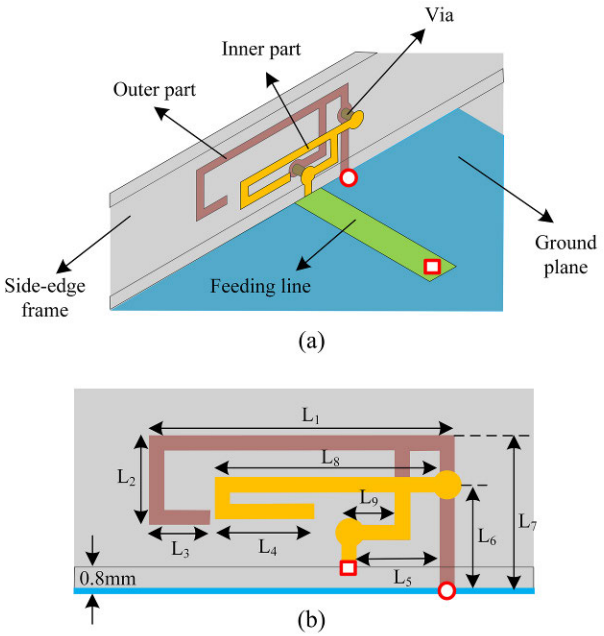

FIGURE 2. Configuration of the proposed dual-mode IFA. (a) Overall view. (b) Side view. Dimensions are $L_1 = 10.3$, $L_2 = 3$, $L_3 = 2$, $L_4 = 4$, $L_5 = 3.3$, $L_6 = 3.6$, $L_7 = 5.3$, $L_8 = 8.2$, $L_9 = 1.5$ (unit: millimeter).

the same port via a 50-ohm microstrip feedline. As can be observed, the proposed dual-mode IFA is composed of two parts which etched on the inner and outer surface of the side-edge frame, respectively. The outer part of the antenna generates the low-order mode at around 3.5 GHz to cover the lower band (3.3-3.6 GHz), while the inner part generates one-quarter-wavelength fundamental mode at around 4.9GHz to fully cover the higher band (4.8-5.0 GHz).

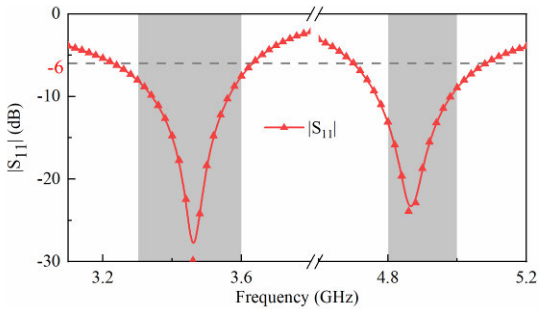

FIGURE 3. Simulated $|S_{11}|$ of the dual-mode IFA (Ant 1).

Fig. 3 shows the simulated reflection coefficients of the proposed dual-mode IFA. It can be seen that the two resonant modes excited by the proposed antenna exhibit good reflection characteristics in both the lower band (3.3-3.6 GHz) and higher band (4.8-5.0 GHz) with reflection coefficient better than −6dB (3:1 voltage standing wave ratio, VSWR). To clearly demonstrate the excitation of these two resonant modes, Fig. 4(a) and (b) shows the surface electric current density distributions at 3.5 and 4.9 GHz, respectively. At 3.5 GHz, a quarter-wavelength current distribution can

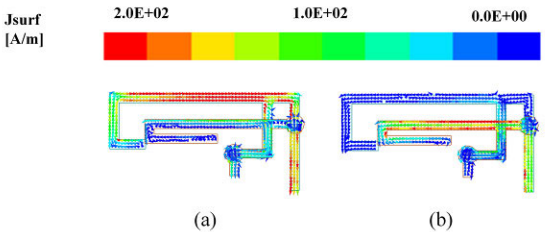

FIGURE 4. Simulated surface current distributions of the dual-mode IFA (Ant 1) at (a) 3.5 GHz and (b) 4.9 GHz.

be observed along the outer part of the proposed antenna. Whereas at 4.9 GHz, the current distribution concentrates along the inner part of the proposed dual-mode IFA. To further illustrate the operating principle, Fig. 5 shows the simulated reflection coefficients as a function of L_2 and L_4. As shown in Fig. 5 (a), by increasing L_2 from 2.7 mm to 3.3 mm, the low-order mode shifts from 3.55 GHz to 3.35 GHz. Similarly, it can be seen in Fig. 5 (b), by increasing L_4 from 3.6 mm to 4.4 mm, the high-order mode shifts from 4.96 GHz to 4.76 GHz.

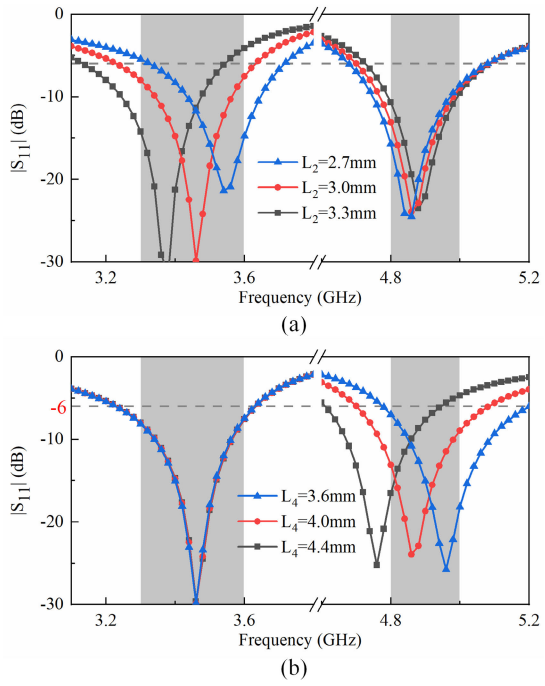

FIGURE 5. Simulated reflection coefficients as a function of (a) L_2 and (b) L_4.

B. TEN-ELEMENT ARRAY WITH DECOUPLING STRUCTURES

In this section, a ten-element array is designed using the proposed dual-mode IFA element. As shown in Fig. 1, Ant 1-Ant 5 and Ant 6-Ant 10 are the mirror images of each other, with respect to the central axis of the system ground plane. Thus, only Ant 1-Ant 5 are analyzed and discussed. To compare the effects of different array

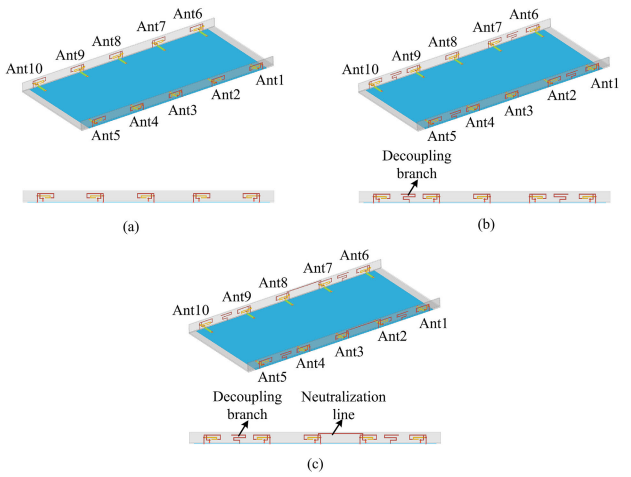

FIGURE 6. Evolution process of the proposed ten-element array. (a) without decoupling structure, (b) with decoupling branches, and (c) the final proposed array.

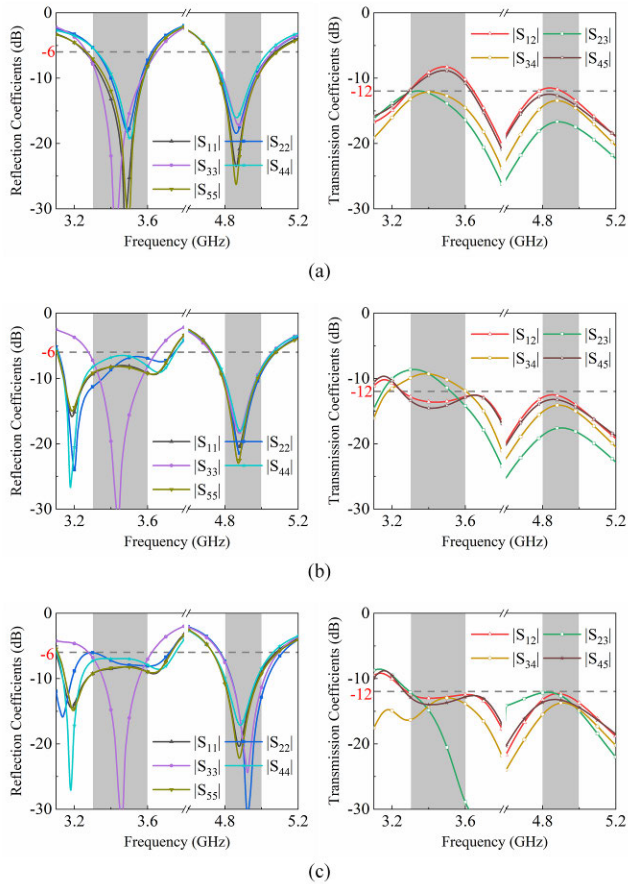

FIGURE 7. Simulated S-parameters of the ten-element array in different cases (a) without decoupling structure, (b) with decoupling branches, (c) the final proposed array.

arrangements, Fig. 6 shows the evolution process of the ten-element array (case 1 and case 2) and the final proposed array.

The simulated S-parameters of case 1 are shown in Fig. 7(a). As can be observed, although all the elements

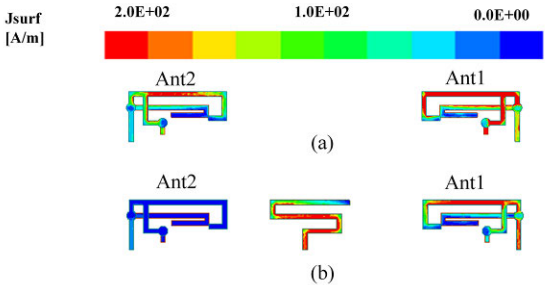

FIGURE 8. Simulated surface current distributions of Ant 1 and Ant 2, (a) without, and (b) with the decoupling branches.

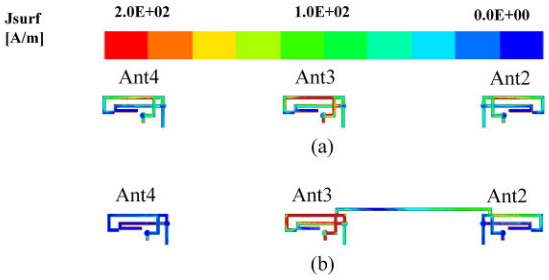

FIGURE 9. Simulated surface current distributions of Ant 2, Ant3 and Ant 4, (a) without, and (b) with the neutralization lines.

can cover the lower band and higher band with the 6-dB impedance bandwidths, the simulated isolations between the antenna pairs (Ant 1 and Ant 2, Ant 4 and Ant 5) are insufficient ($|S_{12}| = -8.3$ dB at 3.5 GHz, $|S_{45}| = -8.8$ dB at 3.5 GHz). In case 2, to enhance the isolations between the antenna pairs, two decoupling branches with the length of a quarter wavelength at 3.5 GHz are introduced between the antenna pairs, as shown in Fig. 6(b). The simulated S-parameters of case 2 are shown in Fig. 7(b). As illustrated in [22], when the decoupling branches are close to the antenna elements, they can work as the parasitic elements because of the coupling from the antenna elements. Therefore, an extra resonance is generated at 3.2 GHz. It can be seen that the isolations ($|S_{12}|$ and $|S_{45}|$) are improved from 8.3 dB to 12 dB. However, the isolation between the Ant2 and Ant3, and the isolation between the Ant3 and Ant4 get worse ($|S_{23}| = -8.7$ dB at 3.3 GHz, $|S_{34}| = -9.3$ dB at 3.4 GHz). To further improve the isolations of the array, the neutralization line is introduced in the middle of Ant2 and Ant3. By adjusting the length of the neutralization line, good S_{23} and S_{34} can be achieved, as shown in Fig. 7(c).

To explain the working mechanism of the decoupling branches and neutralization line, the current distributions are given in Fig. 8 and Fig. 9. Fig. 8 depicts the current distributions of Ant1 and Ant2 (without and with decoupling branch) at 3.5 GHz. When Ant 1 is excited, Ant 2 is terminated with a 50-ohm load. Compared with Fig. 8(a), the surface current distribution on Ant2 in Fig. 8(b) become very weak, which means that lower mutual coupling is realized between Ant1 and Ant2. Fig. 9 shows the current distributions on

Ant2, Ant3 and Ant4 (without and with neutralization line) at 3.5 GHz when Ant 3 is excited and Ant 2 and Ant 4 are terminated. Compared with Fig. 9(a), the surface current distributions at the feeding ports of Ant 2 and Ant4 in Fig. 9(b) are reduced significantly which verifies the decoupling effect of the neutralization line. This is because the strong phase-reversal coupling caused by the intense current on the neutralization line counteracts the original mutual coupling.

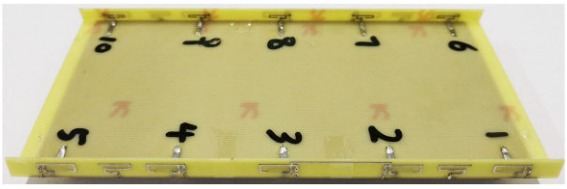

FIGURE 10. Photographs of the fabricated ten-element array.

IV. RESULTS AND DISCUSSION

To validate the above design concept, an antenna prototype of the proposed dual-band ten-element MIMO array with the optimized dimensions was fabricated and measured. Fig. 10 shows the photographs of the fabricated ten-element array. The feeding lines of the antenna elements are directly soldered to 50-ohm connectors at the feed points. In this section, the antenna performances and MIMO performances are presented and discussed in detail.

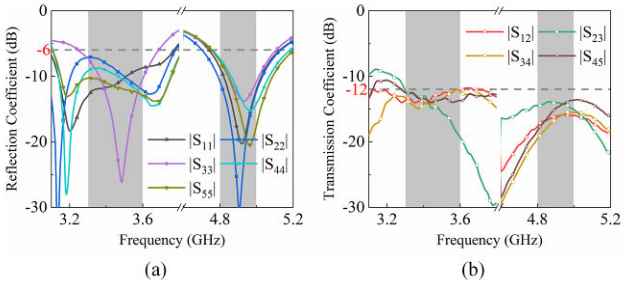

FIGURE 11. Measured (a) reflection coefficients, and (b) transmission coefficients of the proposed antenna array.

A. ANTENNA PROFORMANCE

The measured S-parameters are depicted in Fig. 11. Because of the symmetric layout of the ten-element MIMO array, only the result of Ant 1 to Ant 5 are shown in the figure for brevity. It can be seen that the measured results and simulated results agree well with each other. The slight discrepancies are mainly due to the fabrication tolerances and measurement errors. As shown in Fig. 11(a), for the lower operating band, the measured 6-dB impedance bandwidth is from 3.25 GHz to 3.68 GHz, which can fully cover the desired 3.5-GHz band (3.3-3.6 GHz). For the higher operating band, the measured minimum impedance bandwidth is 4.75-5.12 GHz, which is wide enough for supporting the desired 4.9-GHz band (4.8-5.0 GHz). As depicted in Fig. 11(b), the measured transmission coefficients between the adjacent ports are less than −12 dB, which can ensure good MIMO performance.

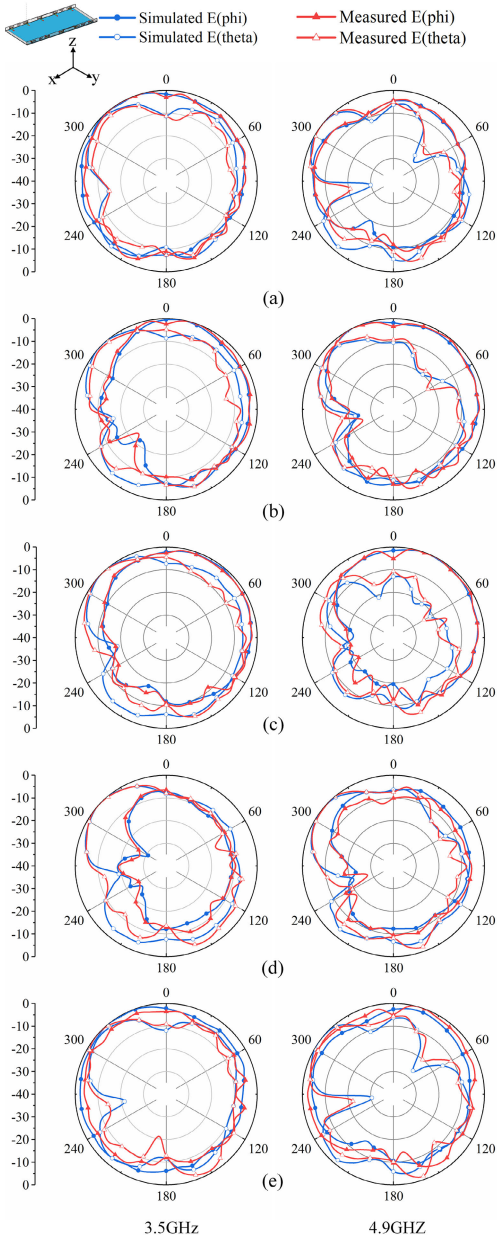

FIGURE 12. Simulated and measured normalized radiation patterns in the yz-plane of the different antenna elements excited separately at 3.5 GHz and 4.9GHz. (a) Ant 1. (b) Ant 2. (c) Ant 3. (d) Ant 4. (e) Ant5.

Fig. 12 shows the simulated and measured radiation patterns in yz-plane at 3.5 GHz and 4.9 GHz, respectively. The simulated 3D antenna radiation patterns of Ant1 to Ant5 are shown in Fig. 13. As can be observed in Figs. 12 and 13, each antenna has a unique radiation pattern and the maximum gains of different antennas point in different directions. Also, the measured radiation patterns show good accordance with the simulated ones at the frequencies of 3.5 GHz and 4.9 GHz. All the radiation performance measurements have

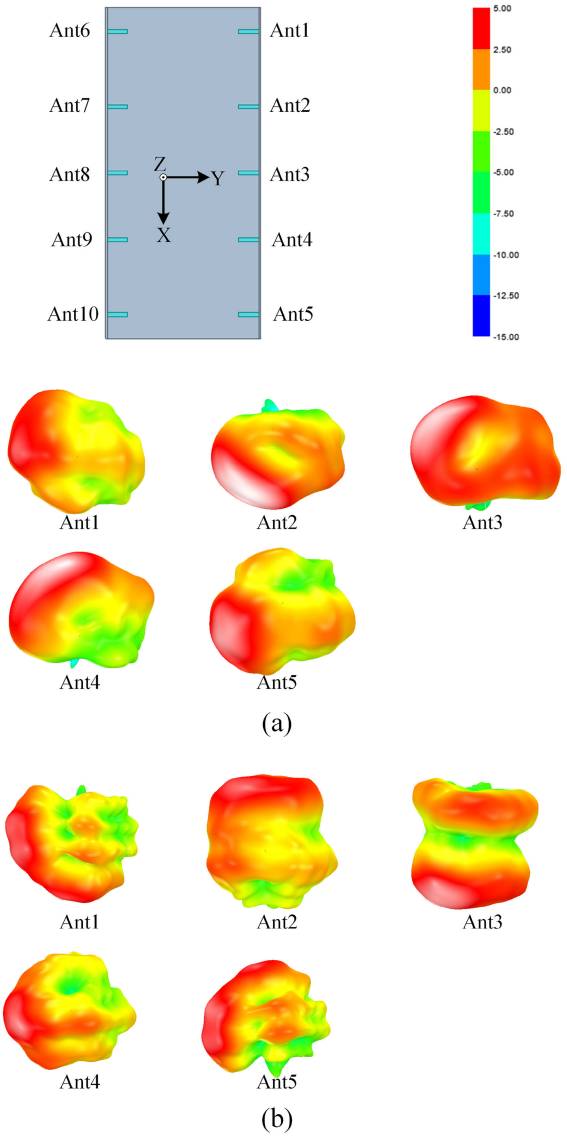

FIGURE 13. Simulated 3D patterns for Ant 1 to Ant 5 at (a) 3.5GHz and (b) 4.9GHz.

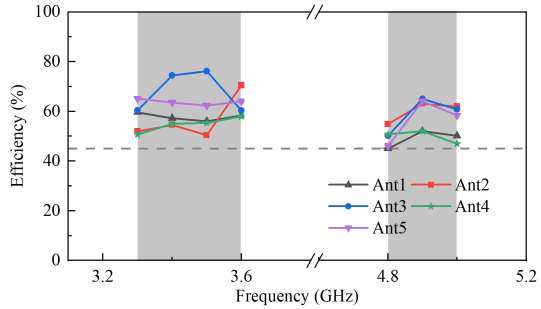

FIGURE 14. Measured antenna efficiencies of the proposed antenna array.

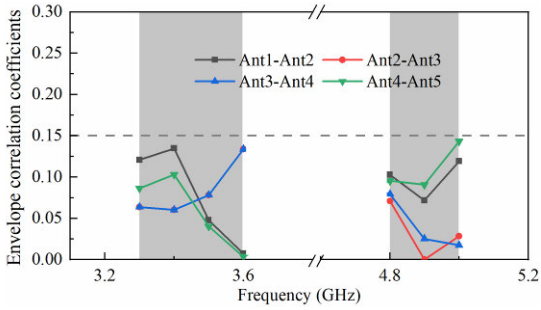

FIGURE 15. Calculated ECCs of the fabricated antenna array.

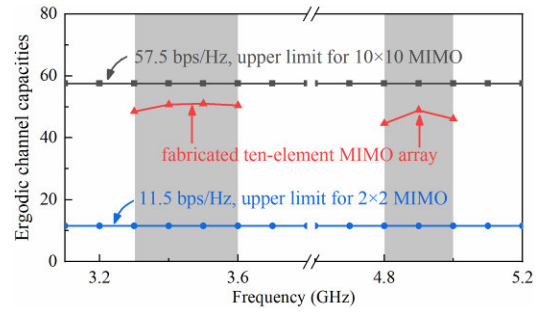

FIGURE 16. Calculated ergodic channel capacities of the fabricated antenna array.

been carried out in a near-field antenna measurement system at Xidian University. The measured antenna efficiencies of the five representative antenna elements (Ant1-Ant5) are presented in Fig. 14. As shown in the figure, the measured antenna efficiencies are about 45%–78% in the 3.5-GHz band, and 45%–65% in the 4.9-GHz band. From the above measured results, it confirmed that the proposed ten-element MIMO array can achieve good array performances that are promising for 5G terminal applications.

B. MIMO PROFORMANCE

In this section, the ECCs and channel capacities will be discussed in detail to evaluate the potential MIMO performance of the proposed array. The calculated ECCs of the elements obtained from the measured radiation patterns are also given in Fig. 15. The obtained ECCs of all the antenna elements are lower than 0.15 in the operating band, which shows a promising diversity performance for a MIMO system. Besides, the calculated ergodic channel capacities of the fabricated ten-element array are shown in Fig. 16. The obtained ergodic channel capacity of the proposed array varies between 46 and 51 bps/Hz. The peak achievable channel capacity (51 bps/Hz) is four times larger than that of an ideal 2 × 2 MIMO (about 11.5 bps/Hz). And it is only 6.5 bps/Hz less than the ideal case of 10 × 10 MIMO (57.5 bps/Hz), thereby showing good multiplexing capability. The channel capacity (CC) in this paper is calculated by the following formulas [23]

$$CC = E\left\{\log_2\left[\det\left(I + \frac{SNR}{n}HH^H\right)\right]\right\} \quad (1)$$

the channel matrix H can be calculated by

$$H = \Phi_r^{1/2} H_w \Phi_t^{1/2} \quad (2)$$

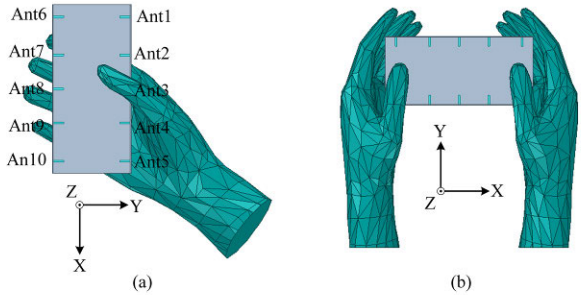

FIGURE 17. Two typical usage scenarios under user's hand operation. (a) single hand model. (b) double hands model.

The receive and transmit antenna correlation matrixes can be expressed as:

$$\Phi_r = {\eta_{total,r}}^{1/2} \rho_r {\eta_{total,r}}^{1/2} \quad (3)$$

$$\Phi_t = {\eta_{total,t}}^{1/2} \rho_t {\eta_{total,t}}^{1/2} \quad (4)$$

The E in equation (1) denotes the expectation with respect to different channel realizations, I is an $n \times n$ identity matrix, SNR is the mean signal-to-noise ratio at the receiving side, n is the number of transmitting antennas, and $(.)^H$ denotes the Hermitian transpose. In this paper, it is assumed that ECC = 0, efficiency = 1 at the transmitting side, while the proposed ten-element array serves as the receiving antenna with envelope correlation coefficient ρ_r and total efficiency $\eta_{total,r}$. And the H_W is a 10×10 matrix, in which the entries are independent identically distributed complex Gaussian random variables.

C. USER'S HAND EFFECTS

It is indispensable to investigate the operating performance of the terminal mobile antenna under the effects of user's hand. So, in this section, the effects of two typical usage scenarios, the single hand model and double hands model, are studied by using the ANSYS High Frequency Structure Simulator (HFSS). The corresponding simulated results under these two hold scenario are shown in Fig. 18. As can be seen, for single hand model, Ants 1, 2, and 6 are far away from the fingers. Because of this arrangement, the S-parameters and efficiencies of these three elements change slightly. In contrast, other elements are very close to the fingers. The efficiencies of these antennas are highly affected owing to the absorption effect of the user's hand. The reflection coefficients are still better than −6 dB across the operation bandwidth for all elements. The isolations are better than 12 dB among all ports except the isolation between Ant7 and Ant8.

For double hands model, a similar phenomenon can be observed in Fig. 18. The reflection coefficients and the isolations remain nearly unchanged. That means the ten-element array can still realize the total coverage of the desired dual-band. Nevertheless, the antenna efficiencies drop to 19% because of the absorption effect of the hands in double hands model.

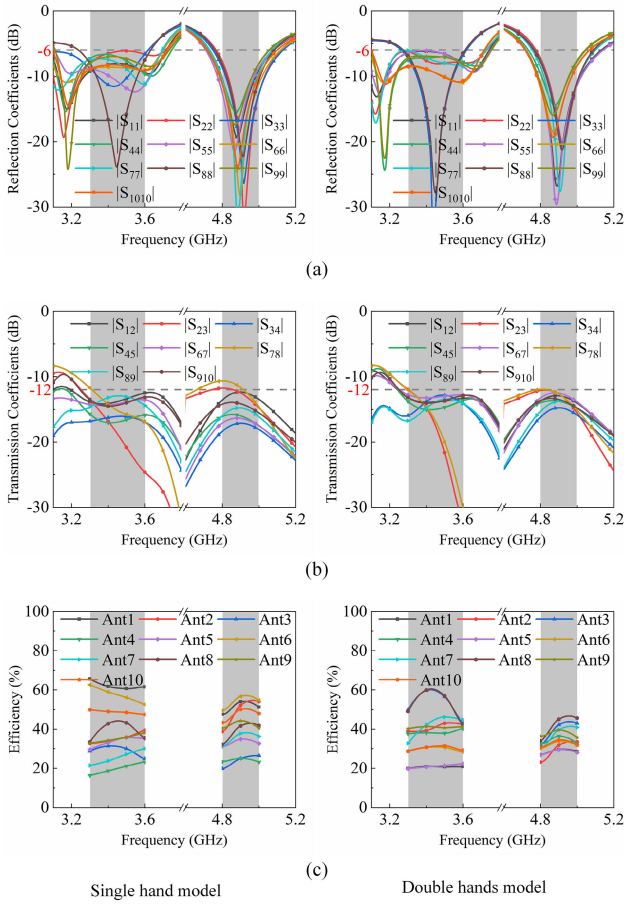

FIGURE 18. Simulated (a) reflection coefficients, (b) transmission coefficients, and (c) antenna efficiencies of the proposed ten-element array in single hand model and double hands model.

D. COMPARISON

Table 1 summarizes the performance comparison between the proposed 5G MIMO antenna array and the recently reported ones. In [2], a four-element MIMO array with high isolation (17 dB) has been designed by using compact self-decoupled antenna structure. However, the channel capacity is extremely lower (18 bps/Hz) compared with the proposed one due to the low MIMO order. In [6], [7], [18], and [19], four higher order MIMO arrays are presented to cover a single band. Compared to these designs, the presented one has an additional operating band at 4.9 GHz (4.8-5.0 GHz) with high isolation and total efficiency. To support dual-band MIMO operation, [14] and [15] proposed two dual-mode antenna elements with the size of 17.0×3.1 mm^2 and 16.0×10.0 mm^2. However, the bulky sizes limit the order of the MIMO array and the channel capacity. The designs in [21] and [23] realized dual-band operation working with a high peak channel capacity close to our proposed array. However, to achieve enough isolation, the antenna elements occupy four sides of the ground plane, leaving no room for 2G/3G/4G antennas. The proposed ten-element MIMO array supports dual-band MIMO operation, and features compact

TABLE 1. Comparison between the proposed design and the referenced antennas for 5G terminal applications.

Ref.	Bandwidth (GHz)	Antenna element size (mm×mm)	Number of occupied sides of the ground	Max distance between elements(mm)	Isolation (dB)	Efficiency (%)	ECC	Peak channel capacity (bps/Hz, 20-dB SNR)	MIMO order
[2]	3.4-3.6	9.4×7.0	2	1.2	>17	>55	<0.1	18 (4×4)	4
[6]	3.4-3.6	10.0×7.0	2	15.0	>10	>40	<0.2	36 (8×8)	8
[7]	3.3-3.6	12.5×4.9	2	17.0	>15	>40	<0.15	35 (8×8)	8
[14]	3.4-3.6, 4.8-5.1	17.0×3.1	2	10.0	>11.5	>40	<0.08	38.5 (8×8)	8
[15]	3.4-3.6, 5.15-5.93	16.0×10.0	2	23.7	>11.2	>51	<0.08	40 (8×8)	8
[18]	3.4-3.8	8.0×3.0	2	20.0	>10	>40	<0.1	47 (10×10)	10
[19]	3.4-3.6	8.0×3.0	2	20.0	>10	>30	<0.35	72 (16×16)	16
[21]	3.4-3.8, 5.15-5.93	16.2×3.0	4	30.2	>11	>42	<0.15	51 (10×10)	10
[23]	3.4-3.6, 5.15-5.93	16.2 × 3.0	4	20.5	>11	>49	<0.1	43.3(8×10)	10
Proposed	**3.3-3.6, 4.8-5.0**	**10.6×5.3**	**2**	**23.0**	**>12**	**>45**	**<0.15**	**51 (10×10)**	**10**

size, high isolation, high efficiency, and low ECC, which can guarantee the MIMO performance with enhanced ergodic channel capacity.

V. CONCLUSION

This paper presents a dual-band ten-element MIMO array based on dual-mode IFAs for 5G terminal applications. Based on the dual-mode characteristics of the proposed element, a dual-band ten-element MIMO array is developed to support the desired 3.5-GHz (3.3-3.6 GHz) band and 4.9-GHz (4.8-5.0 GHz) band. To obtain low mutual coupling within a limited space, neutralization line structures and decoupling branches are introduced between the antenna elements. Isolation of more than 12 dB is achieved in the design. To validate our design concept, the presented dual-band ten-element MIMO array was fabricated and measured. The experimental results show that the proposed antenna can cover the desired sub-6G bands with high isolation and efficiency. Furthermore, the calculated low ECC and large channel capacity indicate that the proposed ten-element MIMO array is a promising candidate for 5G terminal applications.

REFERENCES

[1] Z.-Y. Ren and A.-P. Zhao, "Dual-band MIMO antenna with compact self-decoupled antenna pairs for 5G mobile applications," *IEEE Access*, vol. 7, pp. 82288–82296, 2019.

[2] Z.-Y. Ren, A.-P. Zhao, and S.-J. Wu, "MIMO antenna with compact decoupled antenna pairs for 5G mobile terminals," *IEEE Antennas Wireless Propag. Lett.*, vol. 18, no. 7, pp. 1367–1371, Jul. 2019.

[3] L. Chang, Y. Yu, K. Wei, and H. Wang, "Polarization-orthogonal co-frequency dual antenna pair suitable for 5G MIMO smartphone with metallic bezels," *IEEE Trans. Antennas Propag.*, vol. 67, no. 8, pp. 5212–5220, Aug. 2019.

[4] Q.-G. Chen, H.-W Lin, J.-P. Wang, L. Ge, Y.-J. Li, T.-Q. Pei, and C.-Y.-D. Sim, "Single ring slot-based antennas for metal-rimmed 4G/5G smartphones," *IEEE Trans. Antennas Propag.*, vol. 67, no. 3, pp. 1476–1487, Mar. 2019.

[5] Y.-L. Ban, C. Li, C.-Y.-D. Sim, G. Wu, and K.-L. Wong, "4G/5G multiple antennas for future multi-mode smartphone applications," *IEEE Access*, vol. 4, pp. 2981–2988, 2016.

[6] K.-L. Wong, C.-Y. Tsai, and J.-Y. Lu, "Two asymmetrically mirrored gap-coupled loop antennas as a compact building block for eight-antenna MIMO array in the future smartphone," *IEEE Trans. Antennas Propag.*, vol. 65, no. 4, pp. 1765–1778, Apr. 2017.

[7] W. Jiang, B. Liu, Y. Cui, and W. Hu, "High-isolation eight-element MIMO array for 5G smartphone applications," *IEEE Access*, vol. 7, pp. 34104–34112, 2019.

[8] L. B. Sun, H. Feng, Y. Li, and Z. Zhang, "Compact 5G MIMO mobile phone antennas with tightly arranged orthogonal-mode pairs," *IEEE Trans. Antennas Propag.*, vol. 66, no. 11, pp. 6364–6369, Nov. 2018.

[9] A. Zhao and Z. Ren, "Size reduction of self-isolated MIMO antenna system for 5G mobile phone applications," *IEEE Antennas Wireless Propag. Lett.*, vol. 18, no. 1, pp. 152–156, Jan. 2019.

[10] A. Ren, Y. Liu, and C.-Y.-D. Sim, "A compact building block with two shared-aperture antennas for eight-antenna MIMO array in metal-rimmed smartphone," *IEEE Trans. Antennas Propag.*, vol. 67, no. 10, pp. 6430–6438, Oct. 2019.

[11] Y. Liu, A. Ren, H. Liu, H. Wang, and C.-Y. Sim, "Eight-port MIMO array using characteristic mode theory for 5G smartphone applications," *IEEE Access*, vol. 7, pp. 45679–45692, 2019.

[12] Y.-X. Li, C.-Y.-D. Sim, Y. Luo, and G. L. Yang, "High-isolation 3.5-GHz 8-antenna MIMO array using balanced open slot antenna element for 5G smartphones," *IEEE Trans. Antennas Propag.*, vol. 67, no. 6, pp. 3820–3830, Jun. 2019.

[13] Y. Li, C.-Y.-D. Sim, Y. Luo, and G. Yang, "12-port 5G massive MIMO antenna array in sub-6 GHz mobile handset for LTE bands 42/43/46 applications," *IEEE Access*, vol. 6, pp. 344–354, 2017.

[14] J. L. Guo, L. Cui, C. Li, and B. H. Sun, "Side-edge frame printed eight-port dual-band antenna array for 5G smartphone applications," *IEEE Trans. Antennas Propag.*, vol. 66, no. 12, pp. 7412–7417, Dec. 2018.

[15] J. Li, X. Zhang, Z. Wang, X. Chen, J. Chen, Y. Li, and A. Zhang, "Dual-band eight-antenna array design for MIMO applications in 5G mobile terminals," *IEEE Access*, vol. 7, pp. 71636–71644, 2019.
[16] A.-P. Zhao, and, Z.-Y. Ren, "Wideband MIMO antenna systems based on coupled-loop antenna for 5G N77/N78/N79 applications in mobile terminals," *IEEE Access*, vol. 7, pp. 93761–93771, 2019.
[17] X. Zhang, Y. Li, W. Wang, and W. Shen, "Ultra-wideband 8-port MIMO antenna array for 5g metal-frame smartphones," *IEEE Access*, vol. 7, pp. 72273–72282, 2019.
[18] K.-L. Wong and J. Y. Lu, "3.6-GHz 10-antenna array for mimo operation in the smartphone," *Microw. Opt. Technol. Lett.*, vol. 57, no. 7, pp. 1699–1704, Jul. 2015.
[19] K. L. Wong, J.-Y. Lu, L.-Y. Chen, W.-Y. Li, and Y.-L. Ban, "8-antenna and 16-antenna arrays using the quad-antenna linear array as a building block for the 3.5-GHz LTE MIMO operation in the smartphone," *Microw. Opt. Technol. Lett.*, vol. 58, no. 1, pp. 174–181, Jan. 2016.
[20] M.-Y. Li, Y.-L. Ban, Z.-Q. Xu, J.-H. Guo, and Z.-F. Yu, "Tri-polarized 12-antenna MIMO array for future 5G smartphone applications," *IEEE Access*, vol. 5, pp. 6160–6170, 2018.
[21] Y. Li, C.-Y.-D. Sim, Y. Luo, and G. Yang, "Multiband 10-antenna array for sub-6 GHz MIMO applications in 5-G smartphones," *IEEE Access*, vol. 6, pp. 28041–28053, 2018.
[22] H. Xu, H. Zhou, S. Gao, H. Wang, and Y. Cheng, "Multimode decoupling technique with independent tuning characteristic for mobile terminals," *IEEE Trans. Antennas Propag.*, vol. 65, no. 12, pp. 6739–6751, Dec. 2017.
[23] Y.-X. Li and G.-L. Yang, "Dual-mode and triple-band 10-antenna handset array and its multiple-input multiple-output performance evaluation in 5G," *Int. J. RF Microw. Comput. Aided Eng.*, vol. 29, no. 2, Feb. 2019, Art. no. e21538.

WEI HU (S'09–M'13) received the Ph.D. degree in electromagnetic fields and microwave technology from Xidian University, Xi'an, China, in 2013. From 2013 to 2017, he was a Lecturer with the National Key Laboratory of Antennas and the Microwave Technology, Collaborative Innovation Center of Information Sensing and Understanding, Xidian University, where he is currently an Associate Professor. From 2018 to 2019, he visited the University of Kent, U.K., as an Academic Visitor. He has authored or coauthored over 40 internationally refereed journal articles and has been serving as a reviewer for a number of technical journals and international conferences. His current research interests include multiband and wideband antennas, circularly polarized antennas, MIMO antenna arrays, and wideband wide-scanning phased arrays.

XUEKANG LIU received the B.S. degree from Xidian University, Xi'an, China, in 2016, where he is currently pursuing the M.S. degree in electromagnetic field and microwave technology with the National Laboratory of Science and Technology on Antennas and Microwaves. His current research interests include broadband antennas, multimode antennas, terminal antennas, and omnidirectional antennas.

STEVEN GAO (M'01–SM'16–F'19) received the Ph.D. degree in microwave engineering from Shanghai University, China, in 1999. He is currently a Full Professor and the Chair in RF and microwave engineering, and the Director of Graduate Studies with the School of Engineering and Digital Arts, University of Kent, U.K. He coauthored/co-edited three books [*Space Antenna Handbook* (Wiley, 2012), *Circularly Polarized Antennas* (IEEE-Wiley, 2014), and *Low-Cost Smart Antennas* (Wiley, 2019)], over 300 articles, and ten patents. His research interests include smart antennas, phased arrays, MIMO, reconfigurable antennas, wideband/multiband antennas, satellite antennas, RF/microwave/mm-wave/THz circuits, mobile communications, satellite communications, UWB radars, synthetic-aperture radars, the IoT, and sensors for healthcare. He is a Fellow of Royal Aeronautical Society, U.K., and IET, U.K. He was the General Chair of LAPC 2013 and an Invited Speaker at many conferences. He is currently an Associate Editor of the IEEE TRANSACTIONS ON ANTENNAS AND PROPAGATION and several other international journals, such as *Radio Science*, IEEE ACCESS, *Electronics Letters*, and *IET Circuits, Devices and Systems*, and the Editor-in-Chief for John Wiley and Sons Book Series on *Microwave and Wireless Technologies*. He was a Distinguished Lecturer of the IEEE AP Society.

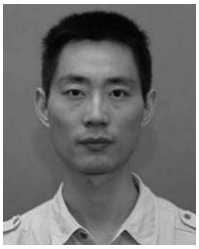

LE-HU WEN received the M.S. degree from Xidian University, Xi'an, China, in 2011. He is currently pursuing the Ph.D. degree with the University of Kent, Canterbury, U.K. His current research interests include multiband base station antenna, mobile terminal antenna, and tightly coupled array.

LONG QIAN received the B.S. degree from Xidian University, Xi'an, China, in 2017, where he is currently pursuing the M.S. degree in electromagnetic field and microwave technology with the National Laboratory of Science and Technology on Antennas and Microwaves. His research interests include mobile terminal antennas and 5G/sub-6GHz MIMO antennas for wireless applications.

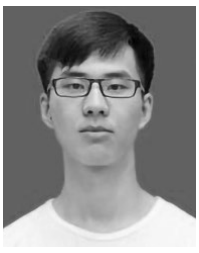

TIANXI FENG received the B.S. degree from Xidian University, Xi'an, China, in 2017, where he is currently pursuing the M.S. degree in electromagnetic field and microwave technology with the National Laboratory of Science and Technology on Antennas and Microwaves. His research interests include circularly polarized antennas and wideband wide-scanning phased arrays.

RUI XU was born in Xi'an, China, in 1989. He received the B.E., master's, and Ph.D. degrees in electronic engineering from Northwestern Polytechnical University, Xi'an, in 2013, 2015, and 2018, respectively. He is currently a Research Associate with the University of Kent, U.K. His current research interests include ultrawideband antennas, waveguide slot antenna arrays, THz antennas, print slot antennas, microstrip antennas, high-gain antennas, and electromagnetic periodic structure.

PENG FEI received the Ph.D. degree in electromagnetic wave and microwave technology from Xidian University, Xi'an, China, in 2013. From August 2013 to May 2016, he was with the Second Academy of China Aerospace Science and Industry Corporation (CASIC), Beijing, China, as a Postdoctoral Fellow. He is currently a Senior Researcher with the Beijing Institute of Radio Metrology and Measurement, Beijing. His research interests include wideband and ultrawideband antennas, passive devices, and microwave imaging.

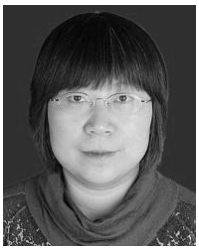

YING LIU (M'09–SM'16) received the M.S. and Ph.D. degrees in electromagnetics from Xidian University, Xi'an, China, in 2001 and 2004, respectively. From 2006 to 2007, she was a Postdoctoral Researcher with Hanyang University, Seoul, South Korea. She is currently a Full Professor and the Director of the National Key Laboratory of Science and Technology on Antennas and Microwaves, Xidian University. She has authored or coauthored over 100 refereed journal articles. She is the author of *Prediction and Reduction of Antenna Radar Cross Section* (Xidian University Press, 2010) and *Antennas for Mobile Communication Systems* (Electronics Industry Press, 2011). Her research interests include antenna theory and technology, prediction, and control of antenna RCS. She is a Senior Member of Chinese Institute of Electronics. She is a reviewer of several international journals and serves as a TPC member or a Session Chair for several IEEE flagship conferences. She was a recipient of the New Century Excellent Talents in University of the Ministry of Education for China, in 2011.